The Influence of Fluid Flow on the Microstructure of Directionally Solidified AlSi-Base Alloys

S. STEINBACH and L. RATKE

To obtain a quantitative understanding of the effect of fluid flow on the microstructure of cast alloys, a technical Al-7 wt pct Si-0.6 wt pct Mg alloy (A357) has been directionally solidified with a medium temperature gradient under well-defined thermal and fluid-flow conditions. The solidification was studied in an aerogel-based furnace, which established flat isotherms and allowed the direct optical observation of the solidification process. A coil system around the sample induces a homogeneous rotating magnetic field (RMF) and, hence, a well-defined flow field close to the growing solid-liquid interface. The application of RMFs during directional solidification results in pronounced segregation effects: a change to pure eutectic solidification at the axis of the sample at high magnetic field strengths is observed. The investigations show that with increasing magnetic induction and, therefore, fluid flow, the primary dendrite spacing decreases, whereas the secondary dendrite arm spacing increases. An apparent flow effect on the eutectic spacing is observed.

I. INTRODUCTION

MOST theoretical models on the development of solidification microstructures are based on diffusive mass transport, whereas convective effects are generally present in most casting processes. Research under microgravity conditions in the last decades has shed light on the importance of fluid flow, and it has become clear that, even in the best experimental setups used on earth, residual flows can change the microstructure and thus hamper a detailed quantitative comparison with theoretical predictions.[1,2] The systematic analysis of convective effects is complicated, as there are many causes for fluid flow (natural convection, solidification shrinkage, stirring, pouring, etc.). When a metallic alloy is solidified, the most frequent morphology is the dendritic microstructure.[3] It is an array of primary, secondary, and sometimes higher-order arms that form a very complex network (Figure 1), where the voids between the dendrite branches are filled by eutectic or intermetallic phases. The problem of microstructure evolution is essentially a multiscale problem: the bulk flow usually occurs on the scale of the sample, but induces effects at the scale of the microstructure. In the last years, efforts were made to study more quantitatively the effects of melt flow on the microstructure evolution during solidification.[4,5,6] The flow effects on the transition from equiaxed to globular microstructure were studied, as were grain refinement and changes in the dendritic network.[7–11]

Summarizing the experimental results obtained so far, one could get the impression that a validated theoretical understanding of the effect of flow on cast structures is still lacking and that experiments designed to trigger theoretical investigations are rare. Therefore, in this article, the effect of fluid flow on the as-cast microstructure of Al-cast alloys is studied under thermally and magnetically controlled convective boundary conditions, to obtain a quantitative understanding of fluid-flow effects on microstructure evolution.

II. EXPERIMENTAL PROCEDURES

In the aerogel-based furnace facility ARTEMIS (Aerogel Technology for Microgravity Solidification)[12,13,14] (DLR, Institute of Materials Physics in Space, Cologne, Germany) cylindrical samples (8 mm in diameter and 120 mm in length) of the composition Al-7 wt pct Si-0.6 wt pct Mg (A357) were solidified directionally from the bottom to the top without and with the influence of a rotating magnetic field (RMF) at a constant temperature gradient of 3 ± 0.1 pct K/mm under vacuum conditions. The solidification velocity v was varied in the range of 0.015 to 0.15 mm/s. The A357 alloy was kindly provided by TITAL (Bestwig, Germany).

A sketch of the ARTEMIS facility is shown in Figure 2. Directional solidification from the bottom to the top heater is carried out by shifting an appropriate temperature profile along the sample. Essential to the facility is the optical control of the process parameters: due to the transparency of the crucible material, silica aerogel,[15,16] the movement of the solidification front during the experiments can be detected with a line charge-coupled device (CCD) camera (256 pixel,

Dr. S. STEINBACH and L. RATKE, Professor, are with the Institut für Materialphysik im Weltraum, DLR, 51170, Köln, Germany. Contact e-mail: sonja.steinbach@dlr.de
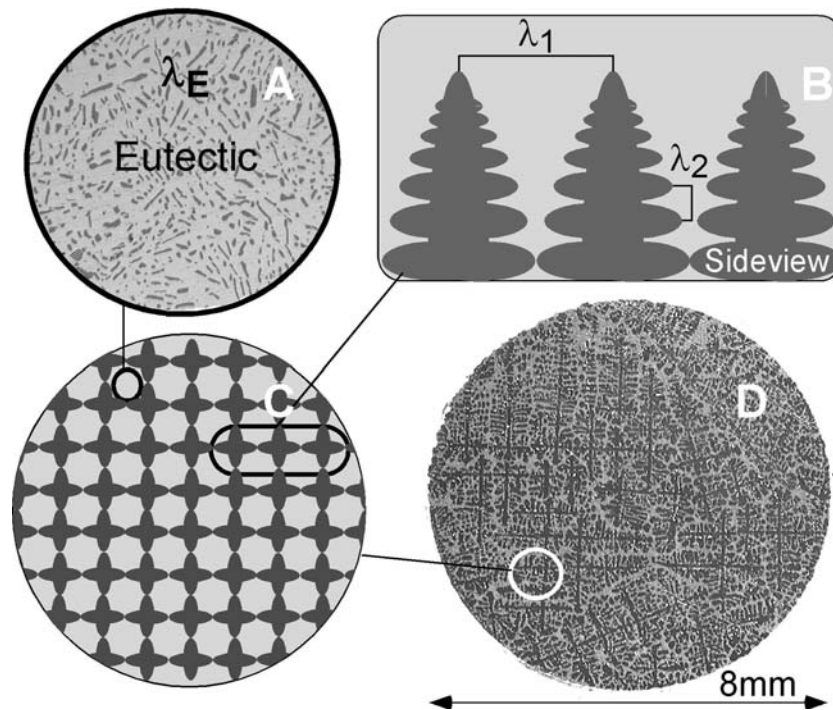
Fig. 1—Definition of primary dendrite spacing λ_1, secondary dendrite arm spacing λ_2, and eutectic spacing λ_E. A: magnified micrograph of the Al-Si interdendritic eutectic of the sample shown in D. D: cross section through an off-eutectic A357 sample showing primary α-Al dendrites lying on a well-defined mesh in a eutectic matrix.

sensitivity 0.9 to 2.2 μm). From these optical measurements, the solidification velocity and the temperature gradient can be determined.[17] Due to the extremely low thermal conductivity of aerogels (~0.05 mW/Km), the isotherms in the sample are flat; due to the aerogel properties, a magnetic field device could be brought very close to the sample. The magnetic field device consists of three pairs of coils around the sample powered by a three-phase current creating a homogeneous RMF; this makes possible the generation of a controlled fluid flow in the melt close to the growing solid-liquid interface. The magnetic induction B_0 was set to either 3 or 6 mT, while the frequency was fixed at 50 Hz. The RMF induces first an azimuthal flow that is proportional to the square root of the magnetic field strength. This flow induces secondary flows in radial and axial directions that are proportional to the fourth power of the magnetic field strength.[18] An increase in the magnetic field strength increases the flow velocity.

The microstructure of the samples was examined on metallographic microsections prepared with a micromilling machine (Reichert-Jung) (Leica Microsystems, Wetzlar, Germany). The microscopic observations were carried out by means of metallographic light microscopes from Wild and Leitz (Leica Microsystems, Wetzlar, Germany). The metallographic preparation of the samples enables the determination of the primary dendrite spacing λ_1, the secondary dendrite arm spacing λ_2, and the eutectic spacing λ_E, with regard to the processing parameters.

The first method for determining the primary spacing is the direct measurement of the distance between two neighboring dendrite centers, because the dendrite
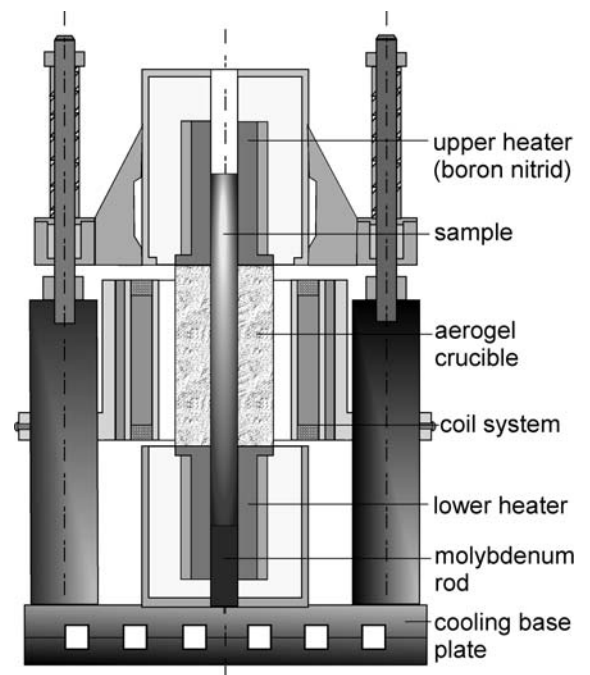

Fig. 2—Simplified computer-aided design drawing of ARTEMIS. The facility utilizes aerogels as a crucible and adiabatic zone material. Due to the extremely low thermal conductivity of aerogels, the isotherms are planar. Due to the transparency of aerogels, especially in the near infrared, the solidification can be observed optically with a line CCD camera.

centers are lying on a well-defined mesh (Figure 1). In the case of samples solidified with the RMF, the spacings were measured in the outer "dendritic ring"
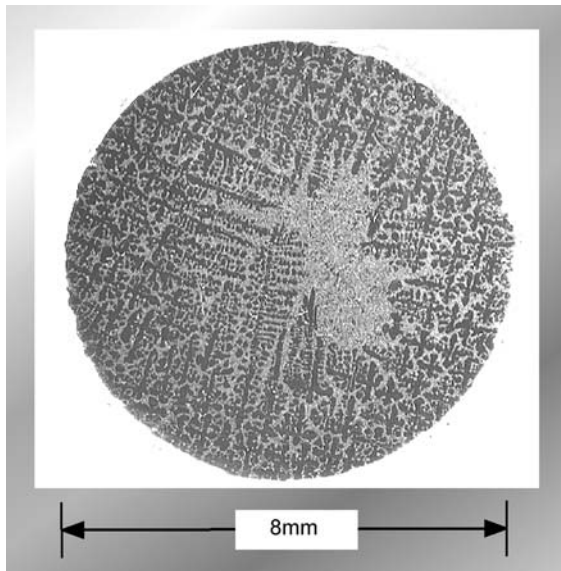
Fig. 3—Cross-sections of an Al-7 wt pct Si-0.6 wt pct Mg sample solidified under the influence of an RMF (G = 3 K/mm, v = 0.015 mm/s, B = 6 mT, and f = 50 Hz). The sample shows a strong Si segregation at its center.

Fig. 4—The radial Si concentration profile of an Al-7 wt pct Si-0.6 wt pct Mg sample (Fig. 3) solidified under the influence of an RMF (G = 3 K/mm, v = 0.015 mm/s, B = 6 mT, and f = 50 Hz). The increase up to the pure eutectic concentration can be observed.

of the samples, excluding the eutectic core region at the center (Figure 3). The second method is the area counting method.[19] In this method, λ_1 is equal to $(A/N)^{0.5}$, where A is the grain area on a cross section, in which the number of primary dendrites N is measured. The first method is used on samples solidified with and without the RMF, and the second method is used only for samples solidified without the RMF.

The secondary dendrite arm spacing λ_2 was measured by averaging the distance between adjacent side branches on the longitudinal section of a primary dendrite, as a function of the length L of the dendrite. The λ_2 is equal to $L/(n-1)$, where n is the number of side branches.

The interlamellar spacing in the nonfaceted-faceted α-AlSi eutectic λ_E was measured by the line intercept method, used also by Grugel and Hellawell.[20,21] On A357 samples solidified without the RMF, the eutectic spacing was measured in the interdendritic region, whereas the spacing of the samples solidified with RMF was measured in the pure eutectic area in the sample center, due to a macrosegregation of Si, as discussed in Section III.

III. RESULTS

Typical microstructures of the ternary alloy A357 solidified without and with forced fluid flow are shown in Figures 1 and 3, respectively. In both cases, a dendritic structure of α-Al with interdendritic α-AlSi eutectic developed. An unexpected effect of the RMF on the A357 alloy is the observed strong macrosegregation. A cross section through a sample solidified with forced convection (Figure 3) shows that a region free of dendrites close to the sample center is a more or less
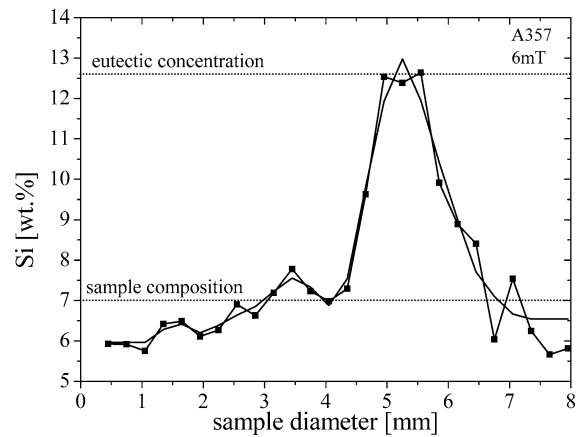
pure α-Al/Si eutectic and, thus, is enriched in silicon from 7 to 12.6 wt pct, as confirmed by energy-dispersive X-ray analysis (EDX) measurements (Figure 4). Usually, these alloys are not prone to segregation, because the density differences between the components are rather small. Although the enrichment of Si in the center is large, the macrosegregation is concentrated only on a small, more or less circular area with a diameter of around 2 mm (Figure 4). The Si concentration in the dendritic ring surrounding the eutectic core is still close to the gross composition. Figure 4 shows that the Si content decreases to 6 wt pct at the periphery. The average Si concentration in this ring can be calculated from the area fraction eutectic to be 6.6 wt pct, and thus is around 6 pct smaller than the gross composition.

The variation in λ_1 with solidification velocity v at a constant temperature gradient G of 3 K/mm for an A357 alloy without and with the RMF (3 and 6 mT at 50 Hz) is shown in Figure 5. The data clearly show, as expected, that an increase in v produces a decrease in λ_1. They also show that the value for the primary stem
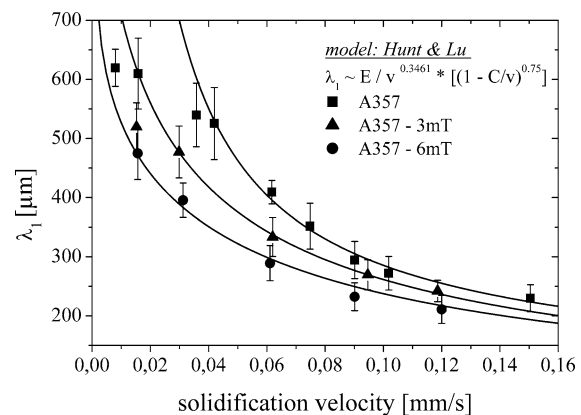

Fig. 5—Primary dendrite spacing λ_1 varying with solidification velocity v of A357 samples solidified without and with RMF (3 and 6 mT at 50 Hz). The measured values are fitted to a dimensionalized model of Hunt and Lu.[27]
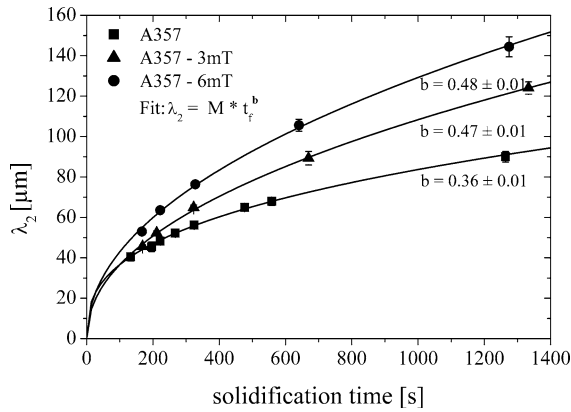
Fig. 6—Secondary dendrite arm spacing λ_2 varying with solidification time t_f of A357 samples solidified without and with RMF (3 and 6 mT at 50 Hz). The measured values are fitted to the well-known coarsening law with an adjustable exponent b.

spacing λ_1 is continuously decreasing with increasing magnetic induction, i.e., increasing flow velocities.

The variation in the secondary dendrite arm spacing with solidification time t_f and magnetic field strength at constant temperature gradient G for the A357 alloys is shown in Figure 6. An increase in solidification time causes an increase in λ_2. It is interesting to note that the secondary dendrite arm spacing without the RMF depends on local solidification time with a power of 0.36 and thus is greater than the well-known value of 1/3.[8,22,23] For the secondary dendrite arm spacing, higher values are obtained with convection, as compared to the case without the magnetic field. In addition to that, a change of the coarsening coefficient from 0.36 to 0.48 is found. The difference between both exponents is far from being a measurement error.

According to the Jackson and Hunt theory,[24] the average lamellar eutectic spacing is inversely proportional to the square root of the solidification velocity v, meaning $\lambda_E^2 v$ is constant. The results for the eutectic spacing (Figure 7) of the A357 alloy show the typical relation between lamellae distance and velocity, i.e.,
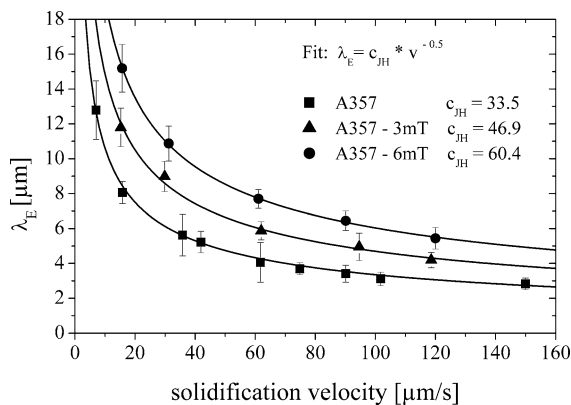

Fig. 7—Lamellar eutectic spacing λ_E varying with solidification velocity v of A357 samples solidified without and with RMF (3 and 6 mT at 50 Hz). The measured values are fitted to the well-known Jackson and Hunt relation,[24] with an adjustable coefficient c_{JH}.

$\lambda_E \approx v^{-0.5}$. The lamellar spacing of the samples solidified with RMF seems to be increased compared to the samples solidified without RMF, under similar local solidification conditions.

IV. DISCUSSION

The experimental results show a strong influence of the forced flow on the microstructural parameters. The main action of the RMF is the generation of an azimuthal rotating flow. The magnetically driven liquid bulk flow creates an interdendritic flow,[18,25] which carries solutally enriched liquid through the mushy zone to the axis of the sample. Thus, a macrosegregation occurs at the center of the sample and pure eutectic solidification finally occurs (Figures 3 and 4). This also means that the isotherms are no longer flat: the eutectic isotherm has a depression in the center of the sample that depends on the amount of RMF stirring. The variation in the Si concentration in the periphery, where the microstructural parameters were measured is, however, not so strong that a large effect of the lower Si content on both primary and secondary dendrite spacing is expected (Figure 4).

Steady-state analysis[26] indicates that a wide range of possible primary spacings could occur during dendritic growth. It is found that a minimum spacing occurs when the dendrite arrays first become stable. The maximum spacing occurs when a tertiary arm becomes a new primary one. The measured values are fitted to a correlation developed by Hunt and Lu.[27] Their complicated expression can be simplified for AlSi alloys using the thermophysical properties of AlSi[28]

$$\lambda_1 \approx \left(\frac{E}{v}\right)^{-0.3416} \left(1 - \frac{C}{v}\right)^{0.75} \qquad [1]$$

with the parameters E and C containing material constants and the solidification velocity v. The data shown in Figure 5 for a zero magnetic field are fitted with Eq. [1]. The agreement is satisfactory. The same expression can be fitted equally well to the data with RMF and, thus, fluid flow. Lehmann et al.[29] have shown with an order-of-magnitude analysis that convection reduces the primary dendrite arm spacing. They assume a flow parallel to the dendrite stem. Such a flow affects perturbations on secondary arms: they are enhanced, as shown by Tong and Beckermann for single dendrites.[4] These perturbations grow opposite to the flow direction and thereby establish a tertiary arm that can become a new primary dendrite; this reduces the primary dendrite stem spacing. A picture as simple as this can explain the observations in general terms, but more detailed considerations and mathematical modeling are required.

The secondary dendrite arm spacing is determined by coarsening processes.[26,27] Independent of the physics of coarsening, all models for secondary dendrite arm spacing predict finally a simple power law expression if diffusive mass transport dominates between the dendrite

arms of the different radii of curvature. These simple models lead to a power law of the type[8,22,23,30]

$$\lambda_2 \approx M \cdot t_f^n \qquad [2]$$

with M a factor containing material constants (diffusion coefficient, Gibbs-Thomson coefficient, eutectic concentration, global concentration, liquidus slope, and segregation coefficient), t_f the solidification time, that is, the time for which the solid and the liquid coexisted, and $n = 1/3$ for diffusive mass transport.

For convective mass transport, Beckermann et al.[4] and Diepers et al.[5] have presented a model that considers the Ostwald ripening of a population of infinitely long cylinders in a flow field, in which they find that flow changes the time dependence of the coarsening rate. Diepers et al. calculated the coarsening rate on two different bases, the time evolution of the mean radius of curvature and the time evolution of the specific surface area. The coarsening rate for pure diffusive transport was found to be $t_f^{1/3}$, irrespective of the calculation basis used. In the presence of flow, the coarsening rate was found to be $t_f^{1/2}$ if calculated on an area basis, and to fall between $t_f^{1/3}$ and $t_f^{1/2}$, if calculated on a curvature basis. As Mullis[31] has shown, the actual effect of fluid flow on the secondary dendrite arm spacing depends on the flow direction, due to the fourfold symmetry of the dendrites in cubic metals, but randomly direct flows should lead to an increase in λ_2. Applying the theoretical considerations of Ratke and Thieringer[32] and Diepers and Beckermann[5] for the RMF case shows a dependence of the secondary arm spacing λ_2 on the solidification time t_f to $\lambda_2 = K\, t_f^{1/2}$. Having a temperature-dependent segregation coefficient should yield values smaller than $1/2$. The values observed in our experiments (Figure 6) would fit into such a picture: the enhanced coarsening in the convective regime causes an increase of the exponent from 0.36 (0 mT) up to 0.48 (6 mT) and, therefore, a change in the kinetics.

The exponent of 0.36 for the λ_2 values of the samples solidified without RMF indicate that, in solutally controlled systems, interdendritic flow by natural convection plays a certain role in the ripening of secondary arms. When evaluating Eq. [2] with a time-dependent temperature profile and with concentration-dependent partition coefficients, the real exponent will be smaller than $1/3$. Observing an exponent larger than that points to an effect of fluid flow, because strong fluid flow can change the kinetics from $1/3$ to $1/2$, and weak flows may lead to intermediate coarsening exponents.[33] Numerical simulation of the ARTEMIS facility[18] shows that there are minor residual convections originating mainly from radial temperature gradients at those regions where the sample leaves the aerogel and enters the furnaces. These small flows with velocities less than 100 μm/s seem to be sufficient for changing the secondary dendrite arm spacing, and thus the coarsening exponent, from 0.33 to 0.36. Experiments performed recently under microgravity conditions with a similar alloy enforced this hypothesis.[34]

The starting point for modern theoretical treatments of eutectic solidification is the seminal article of Jackson and Hunt.[24] During cooperative eutectic solidification, the two phases solidify side by side. The growth is coupled by the diffusion field in front of the growth interface. When the bulk melt differs from the eutectic composition (off-eutectic solidification), as Jackson and Hunt[24] showed, the concentration changes over a distance of D/v, where D is the diffusion coefficient and v is the solidification rate. For alloys of the eutectic composition, the extension of the concentration field is of the order of the eutectic spacing. Whereas D/v is in the experiments performed here is in the range of 10 to 50 μm, λ_E is a decade smaller, in the region of few microns. The eutectic solidification in A357 used in our experiments takes place along the eutectic valley, starting at 576 °C and ending in the ternary eutectic of AlSiMg at 555 °C. Because solidification starts with the crystallization of primary α-Al, the eutectic reaction takes place inside the mushy zone far away from the dendrite tips. At the given temperature gradient, the mushy zone extends approximately 20 mm and the eutectic reaction occurs over a length of 7 mm. It is well known that fluid flow is damped by the dendritic network.[4] Therefore, one cannot expect that convection ahead of the dendrite tips influences the eutectic reaction zone and, thus, λ_E.[35] We do, however, observe an increase of the eutectic spacing with increasing fluid-flow velocity (Figure 7): the spacing doubles from 0 to 6 mT. We think that this increase is an apparent flow effect only.

In Figure 8, the eutectic spacing of the ternary alloy A357 (solidified without RMF) is compared with the spacing of the binary counterpart Al-7 wt pct Si alloy and the pure eutectic Al-12.6 wt pct alloy solidified with the same process parameters. The increase in spacing from the ternary to the binary hypoeutectic AlSi7 alloy can be explained with the Mg content of the technical alloy. The Mg is known for refining the eutectic.[36] However, an increase of the eutectic spacing is also
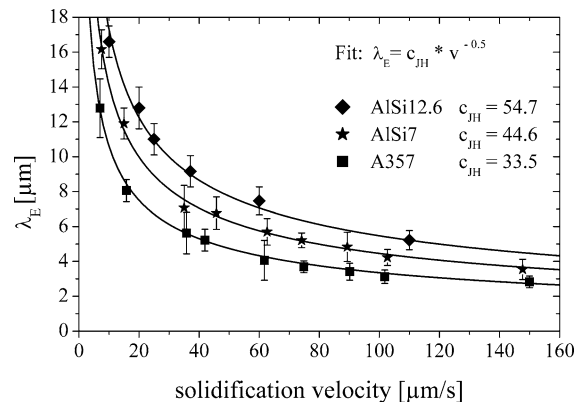

Fig. 8—Lamellar eutectic spacing λ_E varying with solidification velocity v of A357, Al-7 wt pct Si (AlSi7) and pure eutectic Al-12.6 wt pct Si (AlSi12.6) samples solidified under the same conditions. The measured values are fitted to the well-known Jackson and Hunt relation[24] with an adjustable coefficient c_{JH}.

observed, from the hypoeutectic to the pure eutectic alloy.

The total eutectic undercooling is the sum of the curvature undercooling of the eutectic phases and the constitutional undercooling determined by mass transport toward the multiphase interface. For nonfaceted-nonfaceted eutectics, the undercooling is constant along the interface and equal for both phases. The Al-Si eutectic, however, is a nonfaceted-faceted irregular eutectic. For the nonfaceted-phase α-Al, the growth velocity is proportional to the interfacial undercooling, whereas for the faceted-phase Si, it is proportional to the square of the undercooling. Therefore, the Si phase is the leading phase during the growth of the Al-Si eutectic and the interface is nonisothermal. The eutectic growth in an interdendritic region compared with growth of pure eutectic is unique in that, in the interdendritic region, the Al phase already exists and only the undercooling for the Si phase has to be provided. The experimental results in Figure 8 suggest that the required growth undercooling in the case of interdendritic eutectic growth is smaller, as in pure eutectic alloys, and thus the lamellae spacing in hypoeutectic alloys is smaller.

With this explanation and with a comparison of the curves in Figures 7 and 8, the observations in Figure 7 can be explained: for a solidification velocity of 60 μm/s, a eutectic spacing in the Al-12.6 wt pct Si alloy is found to be around 8 μm (Figure 8). For the A357 alloy solidified with 6 mT, more or less the same spacing (Figure 7) is found for the same solidification velocity. This is not astonishing because, as explained previously, the eutectic spacing was measured in the pure eutectic area in the center of the samples solidified with RMF. Therefore, the observed increase of the eutectic spacing with increasing magnetic induction is an apparent fluid-flow effect.

V. CONCLUSIONS

Samples of Al-7 wt pct Si-0.6 wt pct Mg were solidified unidirectionally upward under natural convective and forced-fluid-flow conditions with a constant temperature gradient (3 K/mm) over a wide range of constant solidification velocities v (0.015 to 0.15 mm/s). The melt flow was controlled by time-dependent magnetic fields, allowing the investigation of the effect of convection on the solidification of cast Al alloys. The experimental results show a strong influence of the forced flow on the microstructural parameters; the results can be described with the available theories of Hunt and Lu,[27] Diepers and Beckermann,[5] and Ratke and Thieringer.[32] The scientific results indicate a significant decreasing of the primary dendrite spacing, whereas the secondary dendrite arm spacing increases when a convective solute transport regime is approached. The ripening exponent changes from 1/3 toward a value of 1/2. It is shown that the eutectic spacing depends on the growth region of the eutectic.

REFERENCES

1. M.E. Glicksman, M.B. Koss, L.T. Bushnell, J.C. LaCombe, and E.A. Winsa: *Materials and Fluids under Low Gravity*, Lecture Notes in Physics, L. Ratke, H. Walter, and B. Feuerbacher, eds., Springer Verlag, Heidelberg, 1996, pp. 63–75.
2. S. Steinbach, L. Ratke, and H.D. Masslow: *Proc. 17th Symp. on European Rocket and Balloon Programmes and Related Research*, Sandefjord, Norway, ESA SP-590, 2005, pp. 521–26.
3. W. Kurz and D.J. Fisher: *Fundamentals of Solidification*, Trans Tech Publications, Aedermannsdorf, Switzerland, 1989, pp. 1–316.
4. C. Beckermann, H.-J. Diepers, I. Steinbach, A. Karma, and X. Tong: *J. Comp. Phys.*, 1999, vol. 154, pp. 468–96.
5. H.-J. Diepers, C. Beckermann, and I. Steinbach: *Acta Mater.*, 1999, vol. 47, pp. 3663–78.
6. K. Moenipur and K. Eigenfeld: *Giessereiforschung*, 2004, vol. 50, pp. 103–09.
7. C. Beckermann: *Int. Mater. Rev.*, 2002, vol. 47, pp. 243–61.
8. M.C. Flemings and G.E. Nereop: *Trans. AIME*, 1967, vol. 239, pp. 1449–61.
9. P.A. Davidson and F. Boysan: *Appl. Sci. Res.*, 1987, vol. 44, pp. 241–59.
10. M. Hainke, J. Friedrich, and G. Müller: *J. Mater. Sci.*, 2004, vol. 39, pp. 2011–15.
11. R. Trivedi and W. Kurz: *Int. Mater. Rev.*, 1994, vol. 39, pp. 49–74.
12. J. Alkemper, S. Sous, C. Stöcker, and L. Ratke: *J. Cryst. Growth*, 1998, vol. 191, pp. 252–60.
13. S. Sous and L. Ratke: *Z. Metallkd.*, 2005, vol. 96 (4), pp. 362–69.
14. J. Alkemper, L. Ratke, and S. Sous: *Proc. 4th Decennial Conf. Solidification Processing*, Sheffield, J. Beech and H. Jones, eds., Sheffield University, Sheffield, 1997, pp. 463–67.
15. J. Fricke: *J. Non-Crystal. Solids*, 1992, vol. 145, pp. 1–258.
16. P.H. Tewari, A.J. Hunt, J.G. Lieber, and K. Lufftus: *Aerogels*, J. Fricke, ed., Springer Verlag, Berlin, 1985, p. 142.
17. S. Steinbach and L. Ratke: *Mater. Sci. Forum*, 2006, vol. 508, pp. 491–96.
18. M. Hainke: Ph.D. Thesis, Technical Faculty Erlangen-Nuremberg, Erlangen, Germany, 2004.
19. J.T. Mason, J.D. Verhoeven, and R. Trivedi: *J. Cryst. Growth*, 1982, vol. 59, pp. 516–24.
20. R. Grugel and W. Kurz: *Metall. Trans. A*, 1987, vol. 18A, pp. 1137–42.
21. B. Toloui and A. Hellawell: *Acta Metall.*, 1976, vol. 24, pp. 565–73.
22. N. Whisler and T.Z. Kattamis: *J. Cryst. Growth*, 1972, vol. 15, pp. 20–24.
23. D.H. Kirkwood: *Mater. Sci. Eng.*, 1985, vol. 73, pp. L1–L4.
24. K.A. Jackson and J.D. Hunt: *Trans. AIME*, 1966, vol. 236, pp. 1129–42.
25. P.A. Davidson: *An Introduction to Magnetohydrodynamics*, Cambridge University Press, Cambridge, United Kingdom, 2001, pp. 1–427.
26. J.D. Hunt: *Sci. Technol. Adv. Mater.*, 2001, vol. 2 (1), pp. 147–55.
27. J.D. Hunt and S.Z. Lu: *Metall. Mater. Trans. A*, 1996, vol. A27, pp. 611–23.
28. S. Steinbach: Ph.D. Thesis, RWTH, Aachen, 2005.
29. P. Lehmann, R. Moreau, D. Camel, and R. Bolcato: *J. Cryst. Growth*, 1998, vol. 183, pp. 690–704.
30. M. Rappaz and W.J. Boettinger: *Acta Mater.*, 1999, vol. 47 (11), pp. 3205–19.
31. A.M. Mullis: *J. Mater. Sci.*, 2003, vol. 38, pp. 2517–23.
32. L. Ratke and W.K. Thieringer: *Acta Metall.*, 1985, vol. 33, pp. 1793–1802.

33. L. Ratke and P.W. Voorhees: *Growth and Coarsening: Ostwald Ripening in Material Processing (Engineering Materials)*, Springer Verlag, Berlin, 2002, pp. 1–295.
34. S. Steinbach and L. Ratke: *Micrograv. Sci. Technol.*, 2005, vol. XVI-1, pp. 111–15.
35. W.R. Wilcox and L.L. Regel: *Acta Astronautica*, 1996, vol. 38 (4–8), pp. 511–16.
36. J.E. Gruzleski and B. Closset: *The Treatment of Liquid Aluminum Silicon Alloy*, AFS, Inc, Des Plaines, IL, USA, 1990, ISBN 0874331218.